AIAA JOURNAL
Vol. 43, No. 6, June 2005

Computational Study of Supersonic Base Flow Using Hybrid Turbulence Methodology

Soshi Kawai*
University of Tokyo, Tokyo 113-8656, Japan
and
Kozo Fujii†
Japan Aerospace Exploration Agency, Kanagawa 229-8510, Japan

Large-eddy simulation/Reynolds-averaged Navier–Stokes (LES/RANS) hybrid methodology is applied to a high-Reynolds-number supersonic axisymmetric base flow. Accurate predictions of the base flowfield and base pressure are successfully achieved by using the LES/RANS hybrid methodology with less computational cost than that of pure LES and monotone integrated large-eddy simulation (MILES) approaches. Both the efficiency and reliability of the present LES/RANS hybrid methodology for the prediction of massively separated high-Reynolds-number flows are identified by comparison with the results obtained by LES, MILES, RANS, and the experiments in detail. The LES/RANS hybrid simulation accurately resolves the physics of unsteady turbulent motions, such as shear-layer rollup, large-eddy motions in the downstream region, small-eddy motions inside the recirculating region, and formation of large mushroom-shaped patterns in the end view. Comparison of the results shows that it is necessary to resolve approaching boundary layers and free shear-layer velocity profiles from the base edge correctly for the accurate prediction of base flows. Given the required mesh resolution near solid surfaces for pure LES and MILES at high-Reynolds-number flows, reduction of the computational cost is considerable when using the LES/RANS hybrid methodology. The consideration of a Smagorinsky constant for a compressible flow analysis may suggest that the optimal value of Smagorinsky constant may be larger in the flows with strong compressibility than in incompressible flows.

Nomenclature

A_{VD}	=	van Driest constant
a	=	sonic speed
C_K	=	Yoshizawa model coefficient
C_P	=	local pressure coefficient
C_S	=	Smagorinsky model coefficient
D	=	cylinder base diameter
d_{blend}	=	distance from closest wall to blending position
d_{wall}	=	distance from closest wall
f_{VD}	=	van Driest damping function
M	=	Mach number
Pr_t	=	subgrid-scale turbulent Prandtl number
p	=	static pressure
$\boldsymbol{q}_j^{\mathrm{SGS}}$	=	subgrid-scale heat flux vector
R	=	cylinder base radius
Re	=	Reynolds number
S_{ij}	=	strain rate tensor
T	=	temperature
t	=	time
U_∞	=	freestream velocity
$\langle u\rangle$, $\langle v\rangle$, $\langle w\rangle$	=	time-averaged velocity components
$\boldsymbol{x}_j$	=	coordinate vector
x, θ, r	=	axisymmetric coordinates
$\Gamma(\eta)$	=	blending function
γ	=	ratio of specific heats
Δ_{filter}	=	filter length scale
Δt	=	integration time-step size
Δx, $\Delta\theta$, Δr	=	step size of the grid in x, θ, and r directions
δ_{ij}	=	Kronecker delta
μ_t^{SGS}	=	subgrid-scale turbulent eddy viscosity
ν_t^{SGS}	=	subgrid-scale kinematic eddy viscosity
ρ	=	density
τ_{ij}^{SGS}	=	subgrid-scale stress tensor

Subscript

∞	=	freestream quantity

Superscripts

-	=	spatially filtered quantity
~	=	Favre-filtered quantity
*	=	dimensional quantity
+	=	wall unit quantity

Presented as Paper 2004-0068 at the AIAA 42nd Aerospace Sciences Meeting, Reno, NV, 5–8 January 2004; received 27 September 2004; revision received 28 December 2004; accepted for publication 7 January 2005.

*Research Fellow of the Japan Society for the Promotion of Science, Department of Aeronautics and Astronautics, 7-3-1 Hongo, Bunkyo-ku; kawai@flab.eng.isas.jaxa.jp. Student Member AIAA.

†Professor, Department of Space Transportation Engineering, Institute of Space and Astronautical Science, 3-1-1, Yoshinodai, Sagamihara; fujii@flab.eng.isas.jaxa.jp. Fellow AIAA.

I. Introduction

SUPERSONIC flows past an axisymmetric base are fundamental but important for many engineering problems, such as a projectile, rocket, reentry capsule, aerospike nozzle, reusable launch vehicle, etc. For instance, reusable launch vehicles, especially vertical takeoff and landing type vehicles, while maneuvering in a certain speed range, have large base areas. Their flight regimes include subsonic, transonic, supersonic, and hypersonic speeds, and their aerodynamic characteristics are strongly influenced by the base flowfield along their flight path. Therefore, an accurate estimation of the base flowfield and a resulting force acting on the base are important issues for the design of such vehicles. Furthermore, the knowledge of base flows lies in the ability to control the near wake flow interactions such that base drag can be reduced and vehicle stability and control can be enhanced. Because of the practical importance, various experimental, theoretical, and numerical investigations have been performed for well over a century.

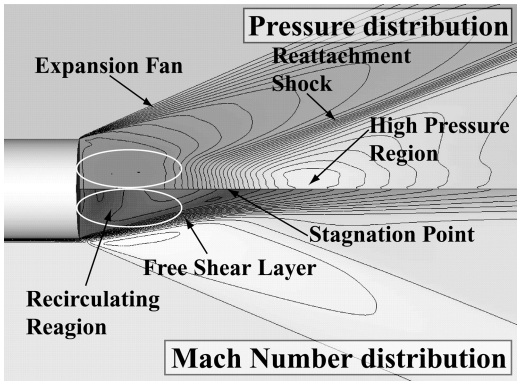

Fig. 1 Schematic of time-averaged axisymmetric base flow.

Extensive experimental investigations of a supersonic base flow have been successfully performed in Refs. 1 and 2, with their experimental facility designed specifically to minimize the effects of a support sting for the study of cylindrical base flows. However, wind-tunnel tests usually use a support sting from the rear of test models. No matter how small in diameter, the presence of a support sting destroys the flow structure behind test models near the wake axis. Most of the wind-tunnel experiments, therefore, usually include some influences of a support sting. Although a few empirical methods have been proposed to compensate the effects of the sting, their reliability is not yet clarified. As a result, an experimental approach is not completely adequate for the estimation of forces acting on the base, and it may be better to combine a computational approach with an experimental approach to establish the reliability of experiments, including sting effects.

There have been various computational fluid dynamics (CFD) studies for the prediction of supersonic base flows. However, most of them used Reynolds-averaged Navier–Stokes- (RANS-) level turbulence models to handle high-Reynolds-number flows. For example, various turbulence models were compared with each other for the application to an axisymmetric truncated plug nozzle.[3] Also, various CFD researchers[4–6] have tried to predict the supersonic axisymmetric base flow described by Herrin and Dutton,[1] who published detailed experimental data of a supersonic axisymmetric base flow at $M_\infty = 2.46$. However, quantitative agreements with the experiment have not yet been achieved by any of the researchers.

Figure 1 presents a computationally obtained schematic showing a time-averaged supersonic base flow at $M_\infty = 2.46$. One may expect that the base flow would be comparatively simple and that prediction of the base flow using CFD would not be difficult. However, that is not the case. Supersonic base flows include large-eddy structures interacting with a shock wave, which produces strong unsteadiness in the flow. This is the main reason that RANS simulations using RANS-level turbulence models do not give satisfactory results.

Thanks to the rapid progress in computers, large-eddy simulation (LES) and monotone integrated large-eddy simulation (MILES) have been applied to complicated flows at high Reynolds numbers in recent years. For the supersonic base flow described by Herrin and Dutton, prediction accuracy has been improved by the unsteady computations using LES[7] and MILES.[8] However, LES and MILES require extremely fine mesh resolution with enormous numbers of grid points near wall regions for high-Reynolds-number flows. In addition, in order to maintain temporal accuracy inside boundary layers, computational time step size is limited by the extremely fine mesh near walls. Because of the restriction in the present computer capability, resolution of the grids near wall regions used in Refs. 7 and 8 was not sufficient to resolve completely the upstream wall-bounded turbulence. In fact, some discrepancies from the experiment were observed, which resulted from the fact that the approaching boundary layer was not fully resolved. However, the influence of the approaching boundary layer on the base flow has not been clarified yet. It may be important to resolve the approaching boundary layer for a base flow analysis even if a separation line is fixed at the base edge. Furthermore, Spalart and Bogue[9] declared dates at which various turbulence approaches became or will become viable for the flow over a wing at useful Reynolds numbers: RANS, 1995; detached-eddy simulation (DES) and LES/RANS hybrid, 2000; LES, 2045; and direct numerical simulation (DNS), 2080. As a result, LES and MILES are not or will not be an easy approach for complex wall-bounded flows at high Reynolds numbers in many engineering problems in present or near-future computer environments. A computational method that can predict base flows within an acceptable computational cost will play a very important role.

To overcome these disadvantages of LES and MILES, LES/RANS hybrid methodology has been proposed in recent years. The LES/RANS hybrid approach applies RANS computation based on Favre-averaged Navier–Stokes equations to the regions near solid surfaces, whereas LES computation based on Favre-filtered Navier–Stokes equations is applicable to the other region that may include massively separated flows. The advantages of the LES/RANS hybrid methodology are that it can alleviate immense grid requirements and resultant severe time-step limitation associated with the small-eddy motions that need to be resolved in wall-bounded regions. Therefore, the hybrid method requires much lower computational cost than that of LES and MILES approaches. Reliability and capability of the hybrid method has been identified for a few applications, such as a supersonic turbulent mixing[10] and a flow around a thin airfoil near stall.[11] However, its reliability is not fully established because it is a comparatively new method, and there are few applications of the hybrid method.

Another approach to simulate massively separated high-Reynolds-number flows is DES.[12–14] DES is a simple modification of Spalart–Allmaras (SA) turbulence model[15] and switches from RANS (SA) to LES-like simulation away from solid surfaces. DES has been applied to several applications, such as a flow past a circular cylinder[16] and a supersonic axisymmetric base flow.[17] In Ref. 17 it is shown that prediction accuracy of a supersonic base flow has been improved compared to RANS (SA) results. As mentioned in Ref. 17, however, DES may not act as pure LES at recirculating regions. In fact, shear-layer rollup has not been well resolved even with a fine grid.

In the present study, the LES/RANS hybrid methodology is applied to the supersonic base flow that was experimentally investigated by Herrin and Dutton. The purposes of this study are to achieve an accurate prediction of the base flow and base pressure by using CFD with lower computational cost than that of LES and MILES approaches and to identify both the efficiency and reliability of the LES/RANS hybrid method for high-Reynolds-number flows by comparison with LES, MILES, and RANS (SA) computational results and the experiments[1,2] in detail. Unknown simulation parameters for the LES/RANS hybrid methodology, such as sensitivities of mesh resolution and the Smagorinsky constant to the supersonic base flow, are also investigated.

II. Mathematical Models

A. Governing Equations

Both Favre-filtered Navier–Stokes equations and Favre-averaged Navier–Stokes equations are derived from the compressible form of Navier–Stokes equations. The details of these derivations are provided in Ref. 18. Both the Favre-filtered and the Favre-averaged Navier–Stokes equations for an ideal gas are nondimensionalized by the density ρ_∞, the speed of sound of the freestream a_∞, and the characteristics length D and are then transformed to a generalized curvilinear coordinate system. Molecular dynamic viscosity is given by Sutherland's law. Favre-averaged Navier–Stokes equations with modeled correlated terms are used for RANS formulation. Favre-filtered Navier–Stokes equations with modeled subgrid-scale (SGS) terms are used for LES formulation. Prandtl number and specific heat ratio are fixed to 0.72 and 1.4, respectively.

B. SGS Modeling

SGS terms in the LES formulation cannot be directly computed. Therefore, SGS models must be introduced to close the system of Favre-filtered Navier–Stokes equations. Various models for the SGS stress tensor τ_{ij}^{SGS} have been proposed to solve incompressible

filtered Navier–Stokes equations. SGS modelings used in the present study for a compressible flow analysis are based on the Smagorinsky model.[19] Additional terms to account for compressibility as shown in Ref. 18 are modeled based on the work of Yoshizawa,[20] Moin et al.,[21] Vreman,[22] and Vreman et al.[23,24]

Smagorinsky eddy viscosity formulation is used to compute τ_{ij}^{SGS} because of its robustness and low computational cost,

$$\bar{\rho}\tau_{ij}^{\mathrm{SGS}} - \tfrac{1}{3}\delta_{ij}\bar{\rho}\tau_{kk}^{\mathrm{SGS}} = -2\bar{\rho}\nu_t^{\mathrm{SGS}}\tilde{S}_{ij} = -2\bar{\rho}C_S^2\Delta_{\mathrm{filter}}^2|\tilde{S}|\tilde{S}_{ij} \quad (1)$$

The SGS eddy viscosity is analogous to the eddy viscosity used in RANS turbulence model and is written as

$$\mu_t^{\mathrm{SGS}} = \bar{\rho}C_S^2\Delta_{\mathrm{filter}}^2|\tilde{S}| \quad (2)$$

The Δ_{filter} in Eq. (1) is chosen to be a characteristic length of a computational grid. This length varies over a grid because of its nonuniform nature. The aspect ratio of the present grid is rather large near the wake axis. Therefore, Deardorff's determination of Δ_{filter} modified by the anisotropy correction of Scotti and Meneveau[25] is introduced. The filter length scaled at each grid point is evaluated by the following formulas:

$$\Delta_{\mathrm{filter}} = (\Delta x\,\Delta\theta\,\Delta r)^{-\frac{1}{3}} f(a_1, a_2) \quad (3)$$

$$f(a_1, a_2) = \cosh\sqrt{(4/27)\left[(\ell_n a_1)^2 - \ell_n a_1\,\ell_n a_2 + (\ell_n a_2)^2\right]} \quad (4)$$

where $f(a_1, a_2)$ is a function of the grid aspect ratios a_1 and a_2. Here, a_1 and a_2 are defined by the two smallest aspect ratios, $a_1 = \Delta_i/\Delta_{\max}$, and $a_2 = \Delta_j/\Delta_{\max}$, $\Delta_{\max} = \max(\Delta x, \Delta\theta, \Delta r)$. $|\tilde{S}|$ in Eq. (1) is defined as

$$|\tilde{S}| = \sqrt{2\tilde{S}_{ij}\tilde{S}_{ij}} \quad (5)$$

Because the isotropic part of the SGS stress tensor $\bar{\rho}\tau_{kk}^{\mathrm{SGS}}$ cannot be computed directly, it must be modeled. In this study, the Yoshizawa model[20] is applied to the computation of the isotropic part of the SGS stress tensor,

$$\bar{\rho}\tau_{kk}^{\mathrm{SGS}} = 2\bar{\rho}\bar{\Delta}_{\mathrm{filter}}^2|\tilde{S}|^2 \quad (6)$$

The eddy diffusivity model is applied to the SGS heat flux term,

$$q_j^{\mathrm{SGS}} = -\frac{\partial}{\partial x_j}\left[\frac{\bar{\rho}\nu_t^{\mathrm{SGS}}}{(\gamma-1)Pr_t M^2}\frac{\partial\tilde{T}}{\partial x_j}\right] \quad (7)$$

where the SGS turbulent Prandtl number Pr_t is fixed to 0.9.

In Ref. 22, it is shown that other SGS terms have negligibly small values compared to the preceding SGS terms. In this study, those terms are neglected based on the works of Moin et al.[21] and Vreman.[22]

For a LES computation in the present study, the following van Driest wall damping function is adopted for the SGS stress tensor τ_{ij}^{SGS} to force the SGS stress to vanish properly in a laminar sublayer portion of the boundary layers,

$$f_{\mathrm{VD}} = 1 - \exp\left(-d_{\mathrm{wall}}^{+}/A_{\mathrm{VD}}\right) \quad (8)$$

where the van Driest constant A_{VD} is 26. Because RANS computation is applied to a laminar sublayer portion of the boundary layers, the wall damping function is not necessary for the computation with the present LES/RANS hybrid methodology.

C. LES/RANS Hybrid Methodology

In the present LES/RANS hybrid methodology, the governing equations in RANS are applied to regions near solid surfaces inside boundary layers, whereas the governing equations in LES are applied to massively separated flow regions. Motivation of the hybrid method is to alleviate the immense grid requirements and severe time step limitation associated with the small eddy motions that need to be resolved in the wall-bounded regions. The Baldwin–Lomax (BL) turbulence model[26] and a compressible form of the Smagorinsky model[19] are used to close the RANS and LES formulation sets. The algebraic models achieve both robustness and low computational cost. These properties often become significant advantages when the LES/RANS hybrid method is applied to engineering problems.

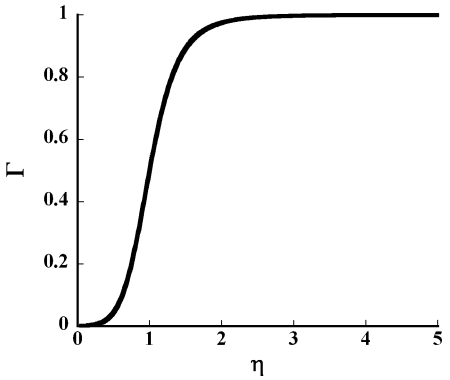

Fig. 2 Behavior of blending function Γ (η).

The following method is used for the blending of the RANS (correlation terms being modeled) and the LES (SGS terms being modeled) formulation sets near the interface of the RANS and LES regions,

$$[\mathrm{LES/RANS\ hybrid}] = \Gamma(\eta)[\mathrm{LES}] + [1-\Gamma(\eta)][\mathrm{RANS}] \quad (9)$$

The blending function $\Gamma(\eta)$ used in the present study is defined as

$$\Gamma(\eta) = \frac{1}{2} + \tanh\left\{\frac{[\alpha(0.2\eta-\beta)]/[0.2(1-2\beta)\eta+\beta]}{2\tanh(\alpha)}\right\} \quad (10)$$

where $\eta = d_{\mathrm{wall}}/d_{\mathrm{blend}}$, $\alpha = 4$, and $\beta = 0.2$. A similar expression is used for the weighting function of inner and outer regions in boundary layers.[27] The blending function $\Gamma(\eta)$ is zero at $\eta = 0.0$ and $\Gamma(\eta) = 0.5$ at $\eta = 1.0$. The parameter α controls the blending width of the LES and RANS regions, where the function changes from 0 to 1, as shown in Fig. 2. The transition from the RANS to LES is smoothly designed around the location specified as d_{blend} in the function (10). To apply the RANS turbulence model to boundary layers, d_{blend} is fixed to the maximum thickness of the boundary layers developing along the lateral surface of a cylindrical body. In the present study, therefore, the fixed value of d_{blend} is used in wall-bounded regions. The blending function $\Gamma(\eta)$ is 0.5 at the location of $d_{\mathrm{wall}} = d_{\mathrm{blend}}$, where the effect of LES and RANS is by halves. The value rapidly increases to 1.0 away from the boundary-layer edge, and d_{blend} is specified from the RANS simulation carried out in advance. In the present study, the value of d_{blend} is set to be $(d_{\mathrm{blend}}^*/D^* =)\ 0.054$.

Time-averaged quantities in RANS formulation are fundamentally different from spatially filtered quantities in LES formulation. However, because of the similar form of RANS and LES formulations, both formulation sets can be solved continuously from a RANS region through a LES region with a single computational method. We are expecting the RANS-to-LES region for a switch from fully modeled stresses given by the turbulence model to resolve stresses that appear when unsteady flows are averaged, as discussed in Ref. 14. The present hybrid method employs the RANS approach to provide the time-averaged flow characteristics of the wall boundary layers. The downstream of the separation is then simulated using the LES. Although the upstream RANS approach does not provide any unsteady turbulent information to the mixing layer, the effects of time-averaged flow momentum are provided to the LES region. Then three-dimensional turbulent fluctuations are developed naturally inside the LES region without any external perturbations. The theoretical contrariety and the lack of turbulent fluctuations in the RANS region (near wall region) are limits of the LES/RANS hybrid methodology. However, successful predictions of qualitative instantaneous flowfield and detailed time-averaged

flow quantities behind the base that we focus on from an engineering viewpoint can be achieved as discussed subsequently in spite of the limitations of the present hybrid method. As a procedure of the hybrid simulation, the BL turbulence model and compressible form of the Smagorinsky model are computed to close the RANS and LES formulations at each time step. Then, both formulation sets are solved continuously from the RANS region through the LES region in time-dependent form.

D. Model Constants

The Smagorinsky constant is not a universal constant in LES simulations of various types of turbulent flows. Here, the constants for SGS modelings are chosen based on previous studies. Vreman et al.[24] derived a relation between C_S and C_K. The following inequality expresses a necessary condition for the realizability of an SGS stress tensor:

$$C_K \geq \left(\sqrt{3}/2\right)C_S^2 \tag{11}$$

Erlebacher et al.[28] derived the model constants based on their DNS results and concluded that $C_S^2 = 0.012$. Yoshizawa[20] proposed that $C_S = 0.16$ and $C_K = 0.0886$ from a two-scale direct interaction approximation. Rogallo and Moin[29] suggested the range of Smagorinsky constant $0.10 \leq C_S \leq 0.24$.

Based on the previous studies, C_K is fixed to 0.0886, and both $C_S = 0.12$ and $C_S = 0.24$ are chosen for the present computations. In this paper, first, the results with $C_S = 0.24$ are discussed mainly for detailed flow analyses. Then, the results with both $C_S = 0.12$ and $C_S = 0.24$ are discussed for the investigation of the flow sensitivity to the Smagorinsky constant. These constants satisfy the inequality (11) and the range of $0.1 \leq C_S \leq 0.24$.

E. Numerical Schemes

A high-order central difference discretization with spectral-like resolution that minimizes dispersive and dissipative numerical errors is preferable for LES. It is shown in Refs. 30 and 31 that the advantage of high-order numerical schemes for a flow analysis behind axisymmetric bodies with a blunt base at supersonic speeds. However, such a central differencing scheme can not be applied directly to the flows, including flow discontinuity such as shock waves, as seen in supersonic base flows. It is shown in Ref. 32 that LES can be carried out with an advection upstream splitting method-[33] (AUSM-) type scheme if sufficient mesh resolution is provided. In this study, governing equations are solved in generalized curvilinear coordinates, where numerical fluxes are evaluated by the high-resolution upwind scheme,[34] which is a family of AUSM type schemes with sufficient mesh resolution. Physical properties at grid interfaces are evaluated by a monotone upwind scheme for conservation law interpolation,[35] based on primitive variables, to achieve third-order space accuracy on an evenly spaced grid. Although the present grid is not an evenly spaced grid, the stretching of the grid is designed to be fairly small at the focused region inside the recirculating region behind the base. Therefore, the space accuracy on the present grid is very close to third order. The viscous terms are evaluated by second-order central differencing. In total, the formal order of accuracy for the present spatial discretization scheme is second order.

The flowfield considered here is essentially unsteady. A lower–upper symmetric Gauss–Seidel (LU-SGS) factorization implicit algorithm[36] with inner iterations is used for time integration to eliminate the errors due to linearization. In this study, second-order temporal accuracy is guaranteed by a three-level backward-differencing formula.

F. Boundary Conditions

It is well known that the generation of a realistic inflow condition is a very sensitive issue in LES. In this study, a compressible flow extension of the rescaling–reintroducing method introduced by Urbin and Knight[37] is used for inflow boundaries. In the method, the flowfield at a downstream station is rescaled and reintroduced at inflow condition as shown in Fig. 3. Fluctuations are automatically generated to the inflow condition through a sequence of operations. Properties at outflow and external boundaries are specified by the zero gradient condition. The solid wall boundary condition at the cylinder surface is treated as no slip, density is extrapolated from an adjacent node, and pressure is defined from the equilibrium condition of the momentum normal to the wall. Properties along a singular line at the wake axis are averaged from the variables at the nodes around the axis. Properties of the boundary in the azimuthal direction are imposed by overlapped nodes' properties.

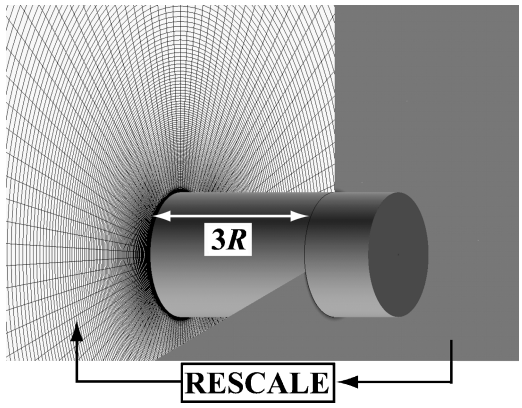

Fig. 3 Rescaling–reintroducing method.

III. Numerical Results

A. Flow Conditions

Flow conditions are based on the experiments of the supersonic axisymmetric base flow of Herrin and Dutton[1] and Bourdon and Dutton.[2] In accordance with the experiments, the freestream Mach number is set to be 2.46, and the Reynolds number based on the cylinder diameter ($D^* = 63.5$ mm) is ($Re = U_\infty^* D^*/\nu^* =$) 2.858×10^6.

B. Computational Setup

1. Temporal Accuracy

For LES computations, it is necessary to resolve unsteady flows both in time and space. Therefore, the local Courant–Friedrichs–Lewy (CFL) number must be kept at a magnitude of order unity (see Ref. 38) or an appropriate number of inner iterations must be adopted for the LU-SGS implicit time-integration method.

To determine a suitable number of inner iterations, four different numbers of inner iterations, 0, 3, 5, and 10, are tested with the grid as shown in Fig. 4, and the influence is investigated. The grid consists of 143 points along the cylinder solid surface, 107 points for the azimuthal direction, and 169 points for the direction normal to the wall. The total number of grid points is approximately 2.54 million. The computational time step is fixed to $\Delta t = \Delta t^* \times a_\infty^*/D^* = 0.005$, where Δt^*, a_∞^*, and D^* represent the dimensional quantities of integration time step, freestream sonic speed, and base diameter, respectively. The local CFL number at the interface of the RANS and LES regions is about 0.9 for the time step. Therefore, the local CFL number in the LES region is less than unity. Time histories of the pressure coefficient at the location of $r/R = 0.5$ on the base surface are shown in Fig. 5. Unsteady behavior of the pressure on the base caused by the unsteady flow inside the recirculating region is clearly shown. For the number of inner iterations of 3, 5, and 10, there is no time delay and the pressure variation is converged, whereas the computation without inner iterations results in a time delay of the pressure variation. From the results, the number of inner iterations of three with $\Delta t = 0.005$ is considered to be sufficient to maintain the temporal accuracy and is used in the present study.

2. Data Processing

The present time step $\Delta t = 0.005$ in the nondimensional time corresponds to $\Delta t^* = 1.37 \times 10^{-6}$ s in the dimensional time, based on the base diameter in the experiment.[1] Time-averaged data are created by averaging flowfields about 30,000 steps (41.1 ms in physical time) of unsteady flow simulations.

Table 1 Grid characteristics

Grid	N_x	N_θ	N_r	N_{total}
Coarse	99	107	123	1.28×10^6
Fine	143	107	169	2.54×10^6
Superfine	181	153	211	5.84×10^6

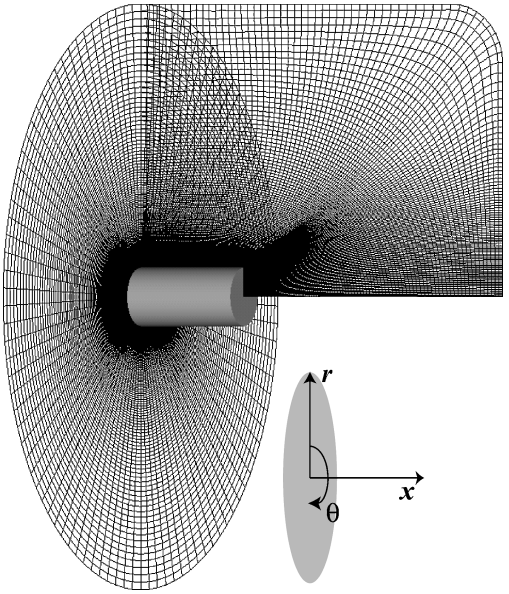

Fig. 4 Computational grid: G2 grid.

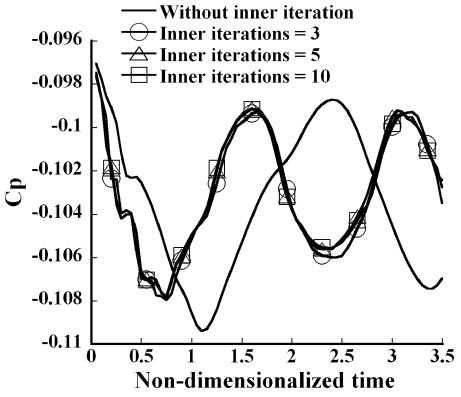

Fig. 5 Time histories of local pressure coefficient on base surface.

3. Sensitivity to Spatial Resolution

Because our purpose is to investigate both efficiency and reliability of the present LES/RANS hybrid methodology for the analyses of high Reynolds number flows, three computational grids are generated for the evaluation of simulation sensitivity to the spatial resolution to clarify an adequate mesh resolution for the hybrid method.

All of the designed grids are topologically O–O type, as shown in Fig. 4. The computational domain extends $4R$ upstream and $10R$ downstream from the base plane, and $9R$ radially from the cylinder lateral surface to the outer boundary. The numbers of grid points are summarized in Table 1, where N_x, N_θ, N_r, and N_{total} represent the number of the grid points in along the body, azimuthal, and wall normal directions and total number of the grid points, respectively. The fine grid consists of 143 points along the cylinder solid surface, 107 points for the azimuthal direction, and 169 points for the direction normal to the wall. The total numbers of grid points for the coarse, fine, and superfine grids are about 1.28, 2.52, and 5.84 million, respectively. The average mesh resolution on the lateral surface of the cylindrical body is about $(\Delta x^+, \Delta\theta^+, \Delta r^+) = (1800, 1400, 1.0)$ in all designed grids.

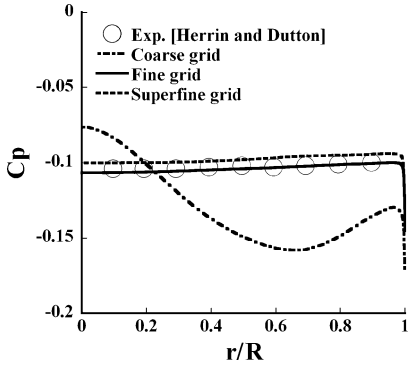

Fig. 6 Time-averaged pressure distributions along base surface obtained with LES/RANS hybrid methodology ($C_S = 0.24$) on each grid system.

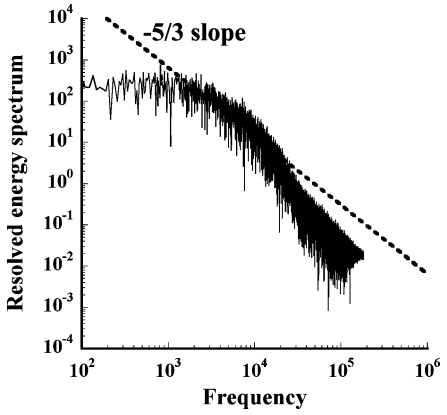

Fig. 7 Resolved energy spectrum in recirculating region obtained by LES/RANS hybrid computation with the fine grid.

Figure 6 shows time-averaged static pressure distributions along the base surface obtained with the LES/RANS hybrid method ($C_S = 0.24$) on each grid system. The result using the coarse grid is clearly underresolved. On the other hand, the results using the fine grid and superfine grid reasonably approach the experiment. The resolved energy spectrum obtained by the present LES/RANS hybrid computation with the fine grid in the recirculating region is shown in Fig. 7. As shown in the frequency resolved spectrum, the resolved scales seem to reach an inertial subrange with close to a $-5/3$ slope. From the results of the grid sensitivity study and resolved energy spectrum, spatial resolution of the fine grid is considered to have an adequate mesh resolution to simulate essential features of the base flow that we focus on with the LES/RANS hybrid methodology. Therefore, the fine grid is used in the present study. The present mesh resolution of the fine grid is similar to the mesh resolutions employed in previous DES[17] and MILES[8] work for the same geometry.

C. Unsteady Flow Structures

Side views of instantaneous vorticity magnitude contours computed by the LES/RANS hybrid and the RANS (SA) methods are shown in Figs. 8 and 9, respectively. As shown in Fig. 8, unsteady shear-layer rollup, large-eddy motions in the downstream region and small-eddy motions inside the recirculating region behind the base are clearly resolved in the LES/RANS hybrid simulation, whereas the DES in Ref. 16 failed to resolve the unsteady shear-layer rollup. On the other hand, the result obtained by the unsteady RANS computation shows little unsteadiness in the flow due to the large turbulent eddy viscosity behind the base edge separation originating from the nature of the SA turbulence model. Therefore, the solution is completely converged in spite of the unsteady simulation. End views of instantaneous Mach number distributions at the $5.0R$ location downstream from the base ($2.0R$ downstream of a stagnation point)

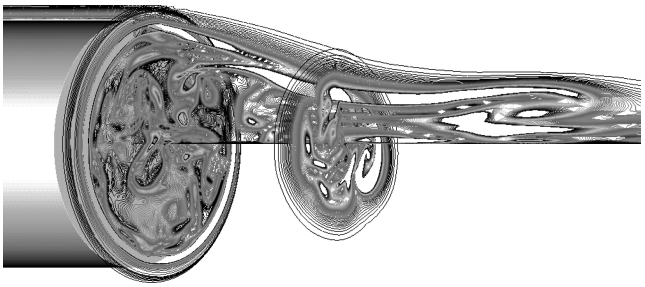

Fig. 8 Instantaneous vorticity magnitude contours, side view: LES/RANS hybrid computation.

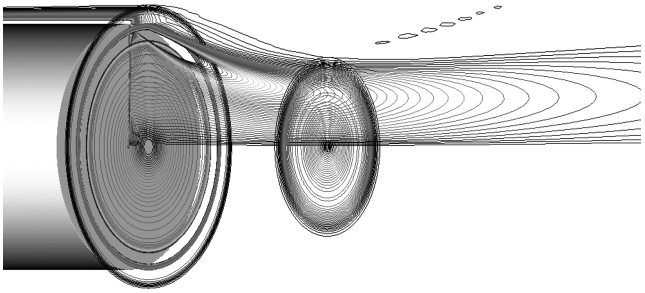

Fig. 9 Instantaneous vorticity magnitude contours, side view: RANS (SA) computation.

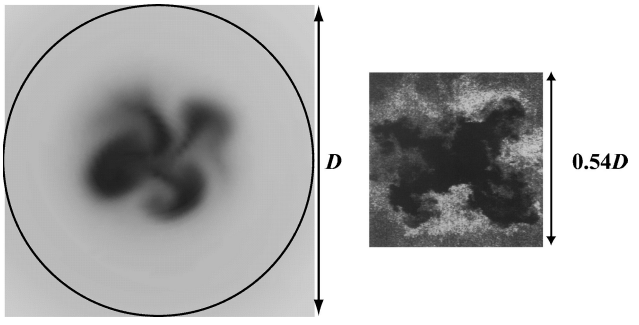

Fig. 10 Instantaneous end view images: a) Mach number contour plots obtained by LES/RANS hybrid computation and b) planar flow visualization image obtained experimentally by Bourdon and Dutton[2] using Mie scattering imaging technique.

computed by the LES/RANS hybrid method (Fig. 10a) and a planar flow visualization image obtained experimentally by Bourdon and Dutton[2] using a Mie scattering imaging technique (Fig. 10b) at almost the same position of the computational result are shown. As for the experimental planar visualization, because condensed ethanol droplets are suspended in the freestream, the high signal shows freestream and the low signal shows recirculation and a wake core region. Therefore, the border of the experimental image in Fig. 10 shows the end view shape of the instantaneous free shear layer. The computed turbulent structure caused by the instability of the shear layer shows the formation of mushroom-shaped patterns in the free shear layer, as shown in Fig. 10. A similar structure is also observed in the experiment of Bourdon and Dutton. These results show the capability of the LES/RANS hybrid methodology for the prediction of unsteady flow features in contrast to unsteady RANS.

D. Boundary-Layer Profile

A comparison of measured and computed boundary-layer velocity profiles on the cylinder lateral surface 1 mm upstream from the base edge is shown in Fig. 11. The present mesh resolution is sufficient to resolve the boundary layer for RANS, but not for LES and MILES. The present LES/RANS hybrid methodology, as well

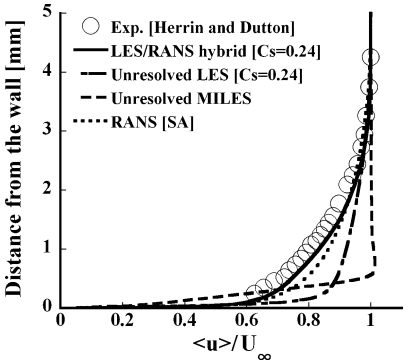

Fig. 11 Boundary-layer velocity distributions at 1 mm upstream from base edge.

as the RANS (SA), predict the boundary-layer profile reasonably well under the current mesh resolution. On the other hand, the LES and MILES fail to resolve the wall-bounded turbulence properly under the present mesh resolution. As a result, thinner boundary-layer profiles compared with the experiment are observed. Note that the difference in the boundary-layer profile influences the wake structures as will be shown in the later sections.

E. Flow Structures Behind Base-Edge Separation

Time-averaged results obtained with the LES/RANS hybrid, LES, MILES, and RANS (SA) computations are discussed. Mach number contour plots computed by the LES/RANS hybrid ($C_S = 0.24$), LES ($C_S = 0.24$), MILES, and RANS (SA) methods are compared with the experiment in Fig. 12. Time-averaged axial and radial velocity distributions at the streamwise stations of $x/R = 0.6299$, 1.2598, and 1.8898 behind the base are compared with the experiment in detail in Figs. 13 and 14. Computed pressures and axial velocity distributions along the wake axis behind the base-edge separation are shown in Figs. 15 and 16, respectively.

In the LES/RANS hybrid computations, time-averaged shear-layer velocity profiles and local Mach number distributions inside the recirculating region agree well with the experiment, as shown in Fig. 12a. Both the axial and radial velocity distributions provide excellent agreement with the experiment, as shown in Figs. 13 and 14. The position and the magnitude of the maximum reverse flow are reasonably well predicted. Flat pressure distribution along the wake axis inside the recirculating region is also observed in the experiments[39] ($M_\infty = 2.0$, 1.92, and 1.85). From the successful prediction of the base flow, it is considered that unsteady computation with the LES/RANS hybrid methodology accurately resolves the physics of unsteady motions.

As for the LES and MILES computations, slightly strong local Mach number distributions compared with the experiment are observed at the regions where maximum reverse flow inside the recirculating region and flow expansion at the base edge are realized, as shown in Figs. 12b and 12c. Both the axial and radial velocity distributions inside the shear layer are overpredicted, as shown in Figs. 13 and 14, because the boundary-layer profiles on the lateral surface of the body have thinner profiles compared with the experiment, as discussed in Sec. III.D. Predicted positions of the free shear layer exist slightly inside at all of the planes compared to the experiment. The discrepancies may be explained by the following mechanisms. The sharp free shear layers with the overpredicted velocity caused by the underprediction of the boundary-layer profile generate from the base-edge separation. The sharp free shear layers meet near the wake axis, and the pressure level of the high-pressure region slightly downstream of the stagnation point becomes higher compared with the result obtained by the LES/RANS hybrid computation, as shown in Fig. 15. Although the lengths of the recirculating region agree well with the experiment, the maximum reverse flow velocity and the flow velocity in the downstream region of the wake are slightly overpredicted (as shown in Fig. 16) due to the strong recirculating and downstream flow induced by the high-pressure region. The strong circulating flow then reduces the static pressure inside the

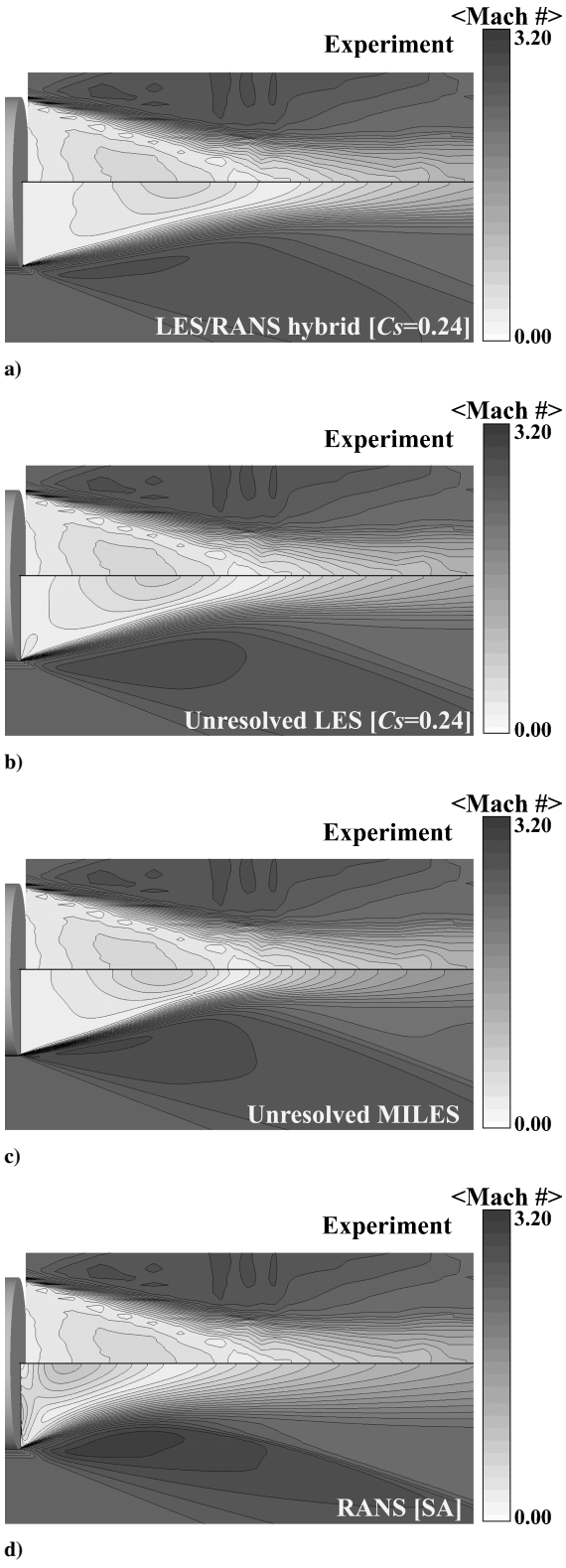

Fig. 12 Mach number contour plots downstream of base-edge separation: a) LES/RANS hybrid vs experiment, b) LES vs experiment, c) MILES vs experiment, and d) RANS (SA) vs experiment.

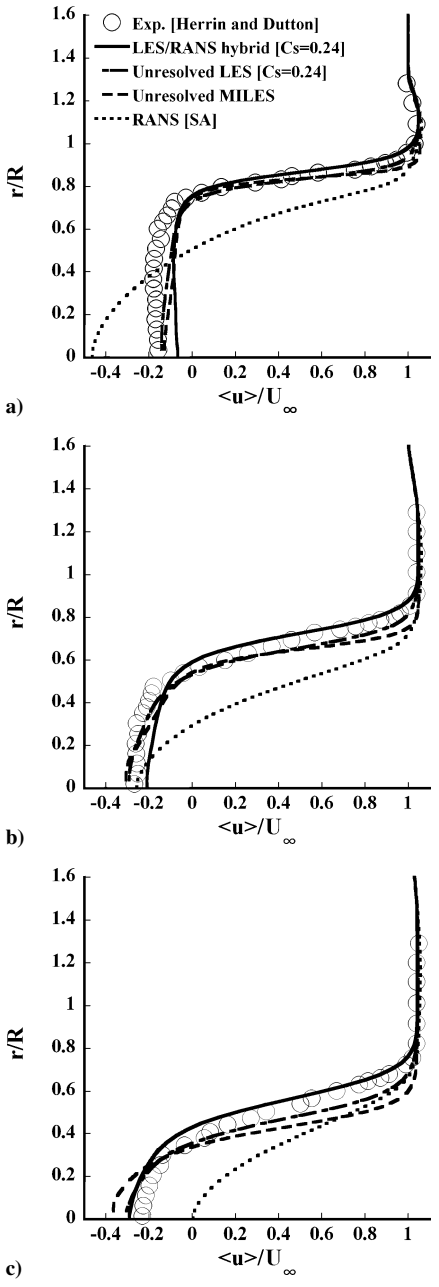

Fig. 13 Comparison of time-averaged axial velocity profiles downstream of base-edge separation: a) $x/R = 0.6299$, b) $x/R = 1.2598$, and c) $x/R = 1.8898$.

recirculating region. To maintain the pressure balance across the free shear layer, expansion from the base edge is promoted, and the free shear layer shifts toward the wake axis. These results indicate that an accurate prediction of supersonic base flows requires an adequate mesh resolution to resolve properly the approaching boundary layer developing along the lateral surface, even if the separation is fixed at the base edge. The capability of the present LES/RANS hybrid methodology for the prediction of wall-bounded high-Reynolds-number flows is significant with respect to the computational cost compared to pure LES or MILES, which would require much more mesh resolution near wall-bounded region.

From the comparison between the results obtained by the LES and MILES, some differences in the growth rate of the time-averaged free shear layer are observed in Figs. 12–14, and the difference of the shear-layer velocity profiles influences the pressure level of the high-pressure region. The width of the free shear layer obtained with the MILES is slightly thinner than that of the LES when the velocity components are compared at the same streamwise station. The difference in the growth rate of the shear layer mainly originates from the explicit (LES) and implicit (MILES) SGS modelings.

In the RANS (SA) computation, free shear layers from the base edge are diffused and curved considerably toward the wake axis compared to the experiment, as shown in Fig. 12d. The recirculating flow becomes smaller and stronger compared with the experiment. The local Mach number distributions have a strong gradient in the axial direction near the base and in the radial direction along the base surface. The discrepancies from the experiment are significant. The

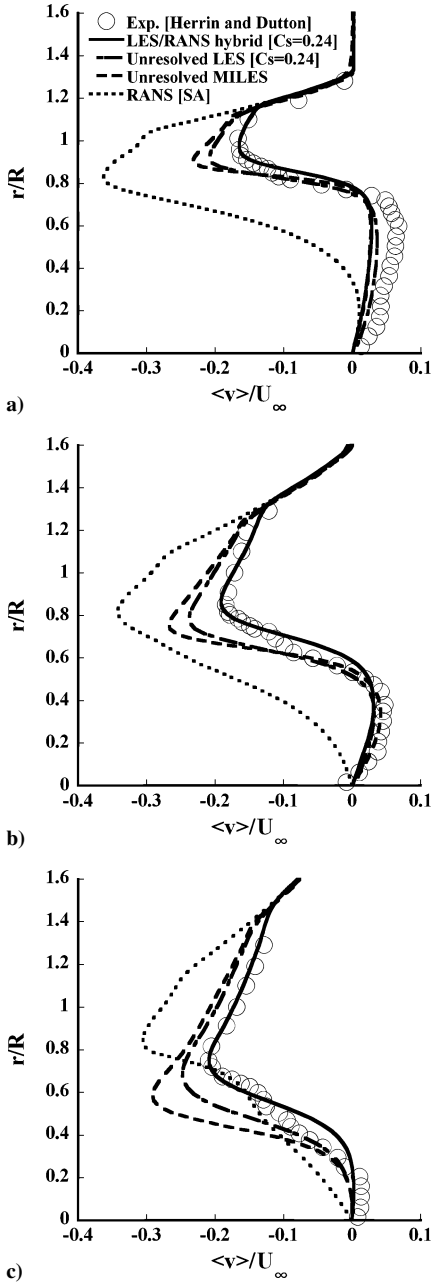

Fig. 14 Comparison of time-averaged radial velocity profiles downstream of base-edge separation: a) $x/R = 0.6299$, b) $x/R = 1.2598$, and c) $x/R = 1.8898$.

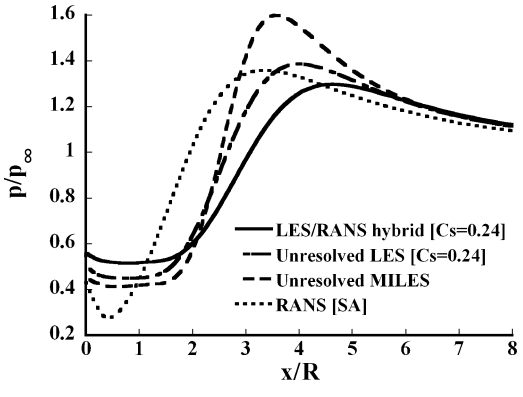

Fig. 15 Time-averaged pressure distributions along wake axis.

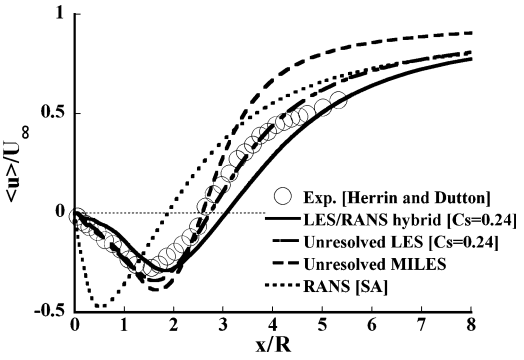

Fig. 16 Time-averaged axial velocity distributions along wake axis.

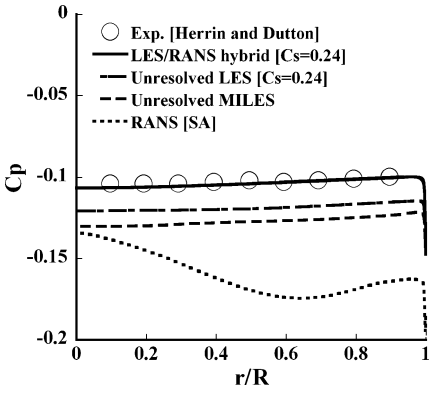

Fig. 17 Time-averaged pressure distributions along base surface.

reason for these discrepancies is considered to come from the large turbulent eddy viscosity behind the base-edge separation induced by the nature of the turbulence model. The large turbulent eddy viscosity considerably diffuses the free shear layer. In fact, the width of the free shear layer is not predicted well at all, and the shear layer exists rather far inside compared to the experiment, as shown in Figs. 13 and 14. The growth rate of the free shear layers determines the location where the free shear layers begin to interfere with each other near the wake axis. Free shear layers meet closer to the base with the increasing growth rate of the free shear layer. Therefore, the free shear layers that are considerably diffused by the strong eddy viscosity meet closer to the base near the wake axis, and the size of the recirculating region is underpredicted, as shown in Fig. 16. The high-pressure region slightly downstream of the stagnation point then appears closer to the base compared to the other computational results, as shown in Fig. 15. The high pressure induces rather strong circulating flow near the base, and the circulating flow rapidly reduces the flow speed to the base because the size of the recirculating region is underpredicted. Relatively low pressure distribution inside the recirculating region is induced by this strong recirculating flow. To maintain the pressure balance, expansion from the base edge is promoted and the free shear layers are curved considerably toward the wake axis.

F. Base Pressure Prediction

Time-averaged base pressure distributions along the base surface are compared with the experiment in Fig. 17. The pressure distribution obtained by the LES/RANS hybrid computation shows excellent agreement with the experiment. Flowfields behind the base-edge separation are essentially unsteady in the LES/RANS hybrid, LES, and MILES computations. Therefore, the base pressures become time dependent. The flat base pressure distributions are obtained when the unsteady flows are time averaged. When the prediction accuracy of the base pressure distributions are compared between the results with the present LES/RANS hybrid methodology and the results with the MILES methodology of Baurle and Tam,[8] better prediction is obtained by using the present LES/RANS hybrid

computation. The prediction accuracy of the base pressure is improved remarkably compared with the result of RANS, with lower computational cost than pure LES or MILES.

The LES and MILES computations show qualitative agreement with the experiment. However, the predicted base pressure distributions are lower than that of the experiment because of the relatively strong recirculating flow induced by the mechanisms discussed earlier. As a result, both the LES and MILES computations failed to give quantitative agreement with the experiment under the present mesh resolution.

As for the RANS (SA) computation, time variation of the base pressure caused by the unsteadiness of the flowfield inside the recirculating region is hardly observed. The predicted base pressure distribution is substantially lower compared to that of the experiment. Even qualitative flat pressure distribution along the base is not predicted. The reverse flow near the wake axis stagnates at the center of the base plane where the region with relatively high pressure appears. Then, the flow is accelerated outward along the base surface, which causes the reduction in pressure in the radial direction. This typical base pressure distribution obtained by RANS computation is caused by the large turbulent eddy viscosity behind the base-edge separation.

G. Sensitivity to Smagorinsky Constant

As for the Smagorinsky model, it is necessary to set the value of C_S in advance. Investigations of the sensitivity of the Smagorinsky constant to the supersonic base flow are performed with two different values of Smagorinsky constant, $C_S = 0.12$ and 0.24. Time-averaged axial velocity distributions along the wake axis with different values of Smagorinsky constant are shown in Fig. 18 and time-averaged axial and radial velocity distributions at the $x/R = 0.6299$, 1.2598, and 1.8898 planes behind the base separation are shown in Figs. 19 and 20. The position of the reattachment moves downstream, and the discrepancy from the experiment is increased as the value of Smagorinsky constant decreases. Discrepancies from the experiment are also observed in the axial and radial velocity distributions with $C_S = 0.12$, whereas the results with $C_S = 0.24$ show excellent agreement with the experiment. The growth rate of the free shear layer is slightly influenced by the value of the Smagorinsky constant. The results obtained with the small value of $C_S = 0.12$ reduces the growth rate of the free shear layer compared with the results obtained with the value of $C_S = 0.24$.

Time-averaged base pressure distributions with different values of Smagorinsky constant are shown in Fig. 21. The base pressure distributions obtained by the result with $C_S = 0.12$ are slightly overpredicted, whereas the result with $C_S = 0.24$ shows excellent agreement with the experiment. The overprediction of the base pressure is caused by the overpredicted size of the recirculating region. However, the difference in the C_p is only 0.012 ($C_P = -0.091$ with $C_S = 0.12$ and $C_P = -0.103$ with $C_S = 0.24$), and the maximum discrepancy from the experiment is not large within the range of $0.12 \leq C_S \leq 0.24$. Note that the prediction accuracy of the base pressure computed with the LES/RANS hybrid methodology is reasonably good around the range of C_S proposed by Rogallo and Moin.

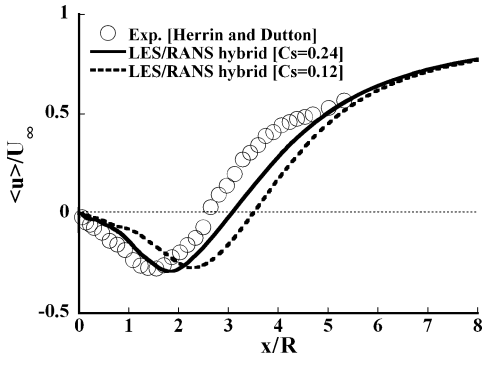

Fig. 18 Time-averaged axial velocity distributions along wake axis.

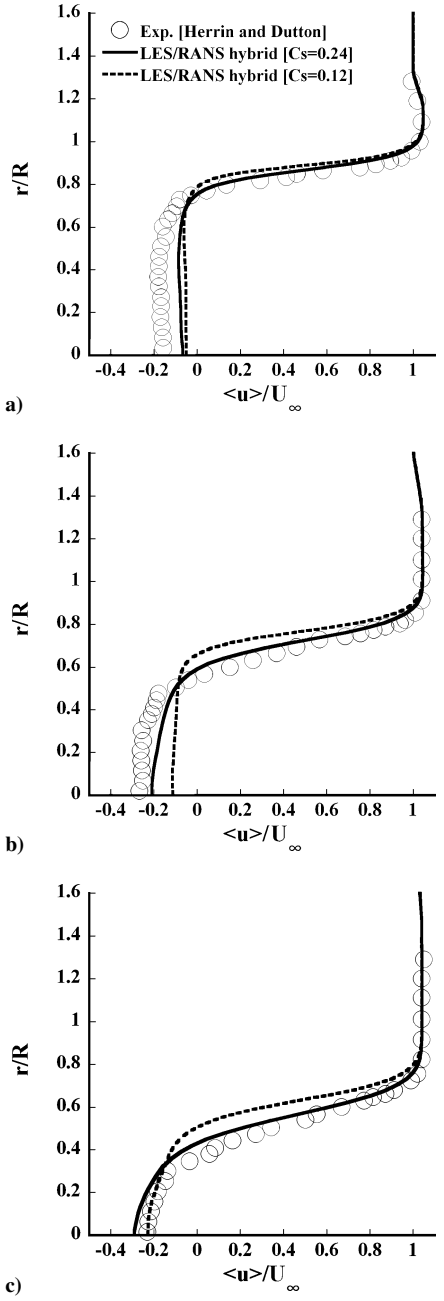

Fig. 19 Comparison of time-averaged axial velocity profiles downstream of base-edge separation with different values of Smagorinsky constant ($C_S = 0.12$ and 0.24): a) $x/R = 0.6299$, b) $x/R = 1.2598$, and c) $x/R = 1.8898$.

From the sensitivity study of the Smagorinsky constant to the base flow, the current explicit SGS modelings behave well with the hybrid method for the prediction of the time-averaged free shear-layer profiles and the base pressure. When the smaller value of the Smagorinsky constant is adopted, the prediction accuracy of the base flowfield decreased. Therefore, the method of simply turning off the SGS turbulent eddy viscosity after the base-edge separation as in the MILES/RANS hybrid approach ($C_S \to 0$) is not considered to behave well for the prediction of the supersonic base flow. The result with the value of Smagorinsky constant of $C_S = 0.24$ shows successful agreement with the experiment, although the value of the Smagorinsky constant around 0.12 is often chosen for investigations of incompressible turbulent mixing.[40] The discrepancy may be explained based on a 2004 private communication with A. Yoshizawa: Generally, strong compressibility suppresses turbulence in turbulent mixing flows, and the turbulent flows become relatively gentle in the flows with strong compressibility. Increasing the value of the

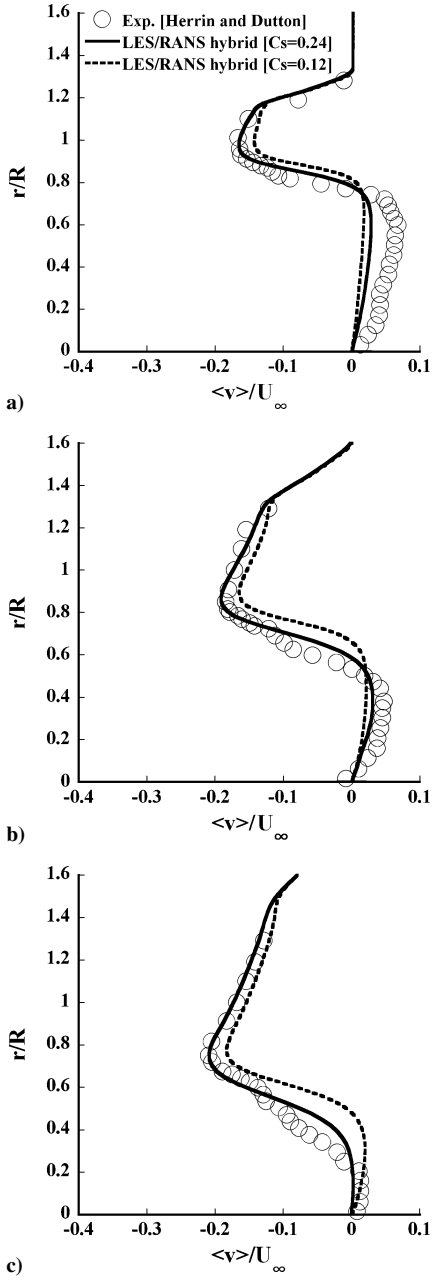

Fig. 20 Comparison of time-averaged radial velocity profiles downstream of base-edge separation with different values of Smagorinsky constant ($C_S = 0.12$ and 0.24): a) $x/R = 0.6299$, b) $x/R = 1.2598$, and c) $x/R = 1.8898$.

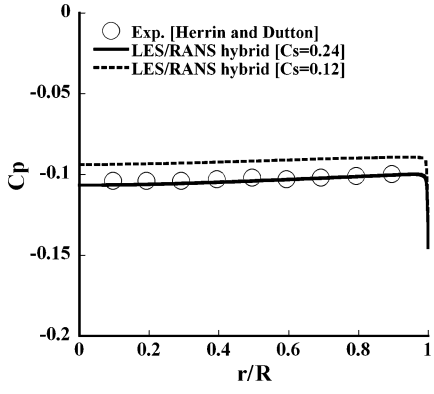

Fig. 21 Pressure distributions along base surface with different values of Smagorinsky constant ($C_S = 0.12$ and 0.24).

Smagorinsky constant has an effect similar to increasing the spatial filter length. [See Eq. (1).] When the spatial filter is increased, turbulence is absorbed into the SGS and the grid-scale turbulence is decreased. As a result, the turbulent flow becomes relatively gentle. Therefore, increasing the Smagorinsky constant for the supersonic base flow analysis is considered to be appropriate. The consideration of the Smagorinsky constant may suggest that the optimal value of the Smagorinsky constant may be larger in flows with strong compressibility than in incompressible flows.

IV. Conclusions

An LES/RANS hybrid methodology was applied to a high Reynolds number supersonic axisymmetric base flow experimentally investigated by Herrin and Dutton. Its efficiency and reliability were investigated by comparison with the results obtained with LES, MILES, RANS (SA), and the experiment in detail. A grid refinement study and the sensitivity of the Smagorinsky constant to the supersonic base flow were also investigated.

Unsteady turbulent motions, such as shear-layer rollup, large-eddy motions in the downstream region, small-eddy motions inside the recirculating region, and the formation of large mushroom-shaped patterns in the end view were properly resolved by the LES/RANS hybrid computations. These results indicated the capability of the LES/RANS hybrid methodology for the prediction of the unsteady flow features in contrast to unsteady RANS.

The base flowfield and base pressure were accurately predicted by the LES/RANS hybrid methodology with lower cost than pure LES and MILES approaches in spite of the theoretical contrariety and the lack of turbulent fluctuations in the RANS region of the present LES/RANS hybrid methodology. As for the base flow simulations, the successful predictions may indicate that the near wall turbulent fluctuations little affect overall flow quantities. As for pure LES or MILES, the required mesh resolution to resolve the approaching boundary layer is at least $(\Delta x^+, \Delta\theta^+, \Delta r^+) = (100, 100, 1.0)$. On the other hand, accurate predictions of the base flowfield and base pressure were successfully achieved by the LES/RANS hybrid computation under the mesh resolution of $(\Delta x^+, \Delta\theta^+, \Delta r^+) = (1800, 1400, 1.0)$. Given the required mesh resolution, the capability of the present LES/RANS hybrid method is significant: The computational cost may be reduced to roughly 250 times lower than that of pure LES and MILES for computation of the same sized domain.

For the prediction of the supersonic base flow, it is necesary to resolve the approaching boundary layer and the free shear-layer growth from the base-edge separation correctly. The LES/RANS hybrid methodology can predict the boundary-layer profile reasonably well, even with the relatively coarse mesh that is sufficient to resolve the boundary layer for RANS, but not for pure LES and MILES. Given the required mesh resolution near the solid surface for pure LES and MILES at high Reynolds flows, the reduction of computational cost is considerable using the computation with the LES/RANS hybrid methodology.

From the sensitivity study of the Smagorinsky constant, current explicit SGS modelings behave well with the present hybrid method for the prediction of the base flowfield and base pressure. The result with the value of Smagorinsky constant of $C_S = 0.24$ showed successful agreement with the experiment. When the smaller value of Smagorinsky constant ($C_S = 0.12$) was adopted, prediction accuracy of the base flowfield decreased. Therefore, the method of simply turning off the SGS turbulent eddy viscosity after the base-edge separation, as in the MILES/RANS hybrid approach ($C_S \to 0$), is not considered to behave well for the prediction of the supersonic base flow. The consideration of the Smagorinsky constant for a compressible flow analysis may suggest that the optimal value of Smagorinsky constant may be larger in flows with strong compressibility than in incompressible flows. The discrepancy from the experiment is not large, within the range of $0.12 \leq C_S \leq 0.24$ with the present LES/RANS hybrid methodology, and the prediction accuracy of base pressure is reasonably good, around the range of C_S proposed by Rogallo and Moin.

In total, the results showed the reliability and capability of the present LES/RANS hybrid methodology for the prediction

of massively separated high-Reynolds-number compressible flows with lower computational cost than that of pure LES and MILES approaches.

Acknowledgments

This work was financed by the Japan Society for the Promotion of Science, Project 16-10764. The first author appreciates their support. The authors are grateful to J. C. Dutton for providing extensive experimental data and to A. Yoshizawa for very helpful discussions on the Smagorinsky constant for a compressible flow analysis.

References

[1]Herrin, J. L., and Dutton, J. C., "Supersonic Base Flow Experiments in the Near Wake of a Cylindrical Afterbody," *AIAA Journal*, Vol. 32, No. 1, 1994, pp. 77–83.

[2]Bourdon, C. J., and Dutton, J. C., "Planar Visualizations of Large-Scale Turbulent Structures in Axisymmetric Supersonic Separated Flows," *Physics of Fluids*, Vol. 11, No. 1, 1999, pp. 201–213.

[3]Schwane, R., Hagemann, G., and Reijasse, P., "Plug Nozzles: Assessment of Prediction Methods for Flow Features and Engine Performance," AIAA Paper 2002-0585, Jan. 2002.

[4]Benay, R., and Servel, P., "Two-Equation $k-\sigma$ Turbulence Model: Application to a Supersonic Base Flow," *AIAA Journal*, Vol. 39, No. 3, 2001, pp. 407–416.

[5]Chuang, C. C., and Chieng, C. C., "Supersonic Base-Flow Computation Using Higher-Order Closure Turbulence Models," *Journal of Spacecraft and Rockets*, Vol. 33, No. 3, 1996, pp. 374–380.

[6]Papp, J. L., and Ghia, K. N., "Application of the RNG Turbulence Model to the Simulation of Axisymmetric Supersonic Separated Base Flows," AIAA Paper 2001-0727, Jan. 2001.

[7]Fureby, C., Nilsson, Y., and Andersson, K., "Large Eddy Simulation of Supersonic Base Flow," AIAA Paper 99-0426, Jan. 1999.

[8]Baurle, A. R., and Tam, J.-C., "Hybrid Simulation Approach for Cavity Flows: Blending, Algorithm, and Boundary Treatment Issues," *AIAA Journal*, Vol. 41, No. 8, 2003, pp. 1463–1480.

[9]Spalart, R. P., and Bogue, R. D., "The Role of CFD in Aerodynamics, Off-Design," *Aeronautical Journal*, Vol. 107, No. 1072, 2003, pp. 322–329.

[10]Georgiadis, J. N., Iwan, J., Alexander, D., and Reshotko, E., "Hybrid Reynolds-Averaged Navier–Stokes/Large-Eddy Simulations of Supersonic Turbulent Mixing," *AIAA Journal*, Vol. 41, No. 2, 2003, pp. 218–229.

[11]Kawai, S., and Fujii, K., "Analysis and Prediction of Thin-Airfoil Stall Phenomena with Hybrid Turbulence Methodology," *AIAA Journal*, Vol. 43, No. 5, 2005, pp. 953–961.

[12]Spalart, P. R., Jou, W.-H., Strelets, M., and Allmaras, S. R., "Comments on the Feasibility of LES for Wings and on the Hybrid RANS/LES Approach," *Advances in DNS/LES, 1st AFOSR International Conference on DNS/LES*, Greyden, Columbus, OH, 1997, pp. 137–147.

[13]Spalart, P. R., "Strategies for Turbulence Modeling and Simulations," *International Journal of Heat and Fluid Flow*, Vol. 21, No. 3, 2000, pp. 252–263.

[14]Spalart, P. R., "Young-Person's Guide to Detached-Eddy Simulation Grids," NASA CR-2001-211032, July 2001.

[15]Spalart, P. R., and Allmaras, S. R., "A One-Equation Turbulence Model for Aerodynamic Flows," AIAA Paper 92-0439, Jan. 1992.

[16]Travin, A., Shur, M., Strelets, M., and Spalart, P. R., "Detached-Eddy Simulations Past a Circular Cylinder," *Flow, Turbulence and Combustion*, Vol. 63, No. 1–4, 1999, pp. 293–313.

[17]Forsythe, J. R., Hoffmann, K. A., Cummings, R. M., and Squires, K. D., "Detached-Eddy Simulation with Compressibility Corrections Applied to a Supersonic Axisymmetric Base Flow," *Journal of Fluids Engineering*, Vol. 124, No. 4, 2002, pp. 991–923.

[18]Kawai, S., and Fujii, K., "Computational Study of a Supersonic Base Flow Using LES/RANS Hybrid Methodology," AIAA Paper 2004-0068, Jan. 2004.

[19]Smagorinsky, J., "General Circulation Experiments with the Primitive Equations, Part 1: The Basic Experiment," *Monthly Weather Review*, Vol. 91, No. 3, 1963, pp. 99–152.

[20]Yoshizawa, A., "Statistical Theory for Compressible Turbulent Shear Flows, with the Application to Subgrid Modeling," *Physics of Fluids*, Vol. 29, No. 7, 1986, pp. 2152–2164.

[21]Moin, P., Squires, K., Cabot, W., and Lee, S., "A Dynamic Subgrid-Scale Model for Compressible Turbulence and Scalar Transport," *Physics of Fluids A*, Vol. 3, No. 11, 1991, pp. 2746–2757.

[22]Vreman, A. W., "Direct and Large-Eddy Simulation of the Compressible Turbulent Mixing Layer," Ph.D. Dissertation, Univ. of Twente, Twente, The Netherlands, Dec. 1995.

[23]Vreman, B., Geurts, B., and Kuerten, H., "Subgrid-modeling in LES of Compressible Flow, Direct and Large-Eddy Simulation 1," Kluwer Academic, Dordrecht, The Netherlands, 1994, pp. 133–144.

[24]Vreman, B., Geurts, B., and Kuerten, H., "Realizability Conditions for the Turbulent Stress Tensor in Large-Eddy Simulation," *Journal of Fluid Mechanics*, Vol. 278, 1994, pp. 351–362.

[25]Scotti, A., and Meneveau, C., "Generalized Smagorinsky Model for Anisotropic Grids," *Physics of Fluids,* Vol. A5, No. 9, 1993, pp. 2306–2308.

[26]Baldwin, B., and Lomax, H., "Thin Layer Approximation and Algebraic Model for Separated Turbulent Flows," AIAA Paper 78-257, Jan. 1978.

[27]Lund, S. T., Wu, X., and Squires, D. K., "Generation of Turbulent Inflow Data for Spatially-Developing Boundary Layer Simulations," *Journal of Computational Physics*, Vol. 140, No. 2, 1998, pp. 233–258.

[28]Erlebacher, G., Hussaini, Y. M., Speziale, G. C., and Zang, A. T., "Toward the Large-Eddy Simulation of Compressible Turbulent Flows," NASA CR-187460, Oct. 1990.

[29]Rogallo, R. S., and Moin, P., "Numerical Simulation of Turbulent Flows," *Annual Review of Fluid Mechanics*, Vol. 17, 1984, pp. 99–137.

[30]Sandberg, R. D., and Fasel, H. F., "Application of a New Flow Simulation Methodology for Supersonic Axisymmetric Wake," AIAA Paper 2004-0067, Jan. 2004.

[31]Sandberg, R. D., and Fasel, H. F., "Instability Mechanisms in Supersonic Base Flows," AIAA Paper 2004-0593, Jan. 2004.

[32]Mary, I., and Sagaut, P., "Large-Eddy Simulation of Flow Around an Airfoil Near Stall," *AIAA Journal*, Vol. 40, No. 6, 2002, pp. 1139–1145.

[33]Liou, M. S., and Steffen, C. J., Jr., "A New Flux Splitting Scheme," *Journal of Computational Physics*, Vol. 107, No. 1, 1993, pp. 23–39.

[34]Shima, E., and Jounouchi, T., "Role of CFD in Aeronautical Engineering (No. 14)-AUSM Type Upwind Schemes," *Proceedings of the 14th NAL Symposium on Aircraft Computational Aerodynamics*, National Aeronautical Lab., Tokyo, 1997, pp. 7–12.

[35]van Leer, B., "Towards the Ultimate Conservative Difference Scheme 5. A Second-Order Sequel to Godunov's Method," *Journal of Computational Physics*, Vol. 32, 1979, pp. 101–136.

[36]Yoon, S., and Jameson, A., "Lower–Upper Symmetric-Gauss–Seidel Method for the Euler and Navier–Stokes Equations," *AIAA Journal*, Vol. 26, No. 9, 1988, pp. 1025, 1026.

[37]Urbin, G., and Knight, D., "Large-Eddy Simulation of a Supersonic Boundary Layer Using an Unstructured Grid," *AIAA Journal*, Vol. 39, No. 7, 2001, pp. 1288–1295.

[38]Choi, H., and Moin, P., "Effects of the Computational Time Step on Numerical Solutions of Turbulent Flow," *Journal of Computational Physics*, Vol. 113, No. 1, 1994, pp. 1–4.

[39]Delery, J., and Sirieix, M., "Base Flows Behind Missiles," *Cycle of Conferences AGARD LS-98 on Aerodynamic of Missiles*, TP 1979-14E, AGARD, 1979, pp. 1–70.

[40]Hamba, F., "Large Eddy Simulation of a Turbulent Mixing Layer," *Journal of the Physical Society of Japan*, Vol. 56, Aug. 1987, pp. 2721–2732.

P. Givi
Associate Editor